

# Deep Direct Visual Servoing of Tendon-Driven Continuum Robots

Ibrahim Abdulhafiz<sup>1</sup>, Ali A. Nazari<sup>2,\*</sup>, Taha Abbasi-Hashemi<sup>1</sup>, Amir Jalali<sup>2</sup>,  
Kourosh Zareinia<sup>2</sup>, Sajad Saeedi<sup>2</sup>, and Farrokh Janabi-Sharifi<sup>2</sup>

**Abstract**—Vision-based control has found a key place in the research to tackle the requirement of the state feedback when controlling a continuum robot under physical sensing limitations. Traditional visual servoing requires feature extraction and tracking while the imaging device captures the images, which limits the controller’s efficiency. We hypothesize that employing deep learning models and implementing direct visual servoing can effectively resolve the issue by eliminating the tracking requirement and controlling the continuum robot without requiring an exact system model. In this paper, we control a single-section tendon-driven continuum robot utilizing a modified VGG-16 deep learning network and an eye-in-hand direct visual servoing approach. The proposed algorithm is first developed in Blender using only one input image of the target and then implemented on a real robot. The convergence and accuracy of the results in normal, shadowed, and occluded scenes reflected by the sum of absolute difference between the normalized target and captured images prove the effectiveness and robustness of the proposed controller.

## I. INTRODUCTION

Continuum robots (CRs) are inspired by biological appendages such as octopus arms, elephant trunk, and monkey’s tail [1]. These robots are made of soft, elastic, compliant, and lightweight materials together with some rigid elements [2], which lead to the ability to manipulate geometrically complex objects and work in unstructured and confined environments [3]. They can smoothly move by elongation, contraction, and bending. Compared to their rigid counterparts, CRs are better for manipulating deformable objects, working in confined and unstructured spaces, and safely operating close to humans [4]. These compliant robots can be actuated intrinsically, by employing pneumatic and hydraulic actuators, or extrinsically, by utilizing concentric tubes and tendons [5]. Concentric-tube CRs [6], [7] and tendon-driven CRs have typically small diameter-to-length ratios [5]. The small ratio enables them to reach highly confined spaces as well as technically inspect unstructured environments [8].

Affected by the intrinsic compliance and the high number of degrees of freedom (DOFs), the control of CRs has been a challenge since their emergence. A set of control methods are based on the mathematical modeling of CRs

\*Corresponding author; Email: [ali.nazari@ryerson.ca](mailto:ali.nazari@ryerson.ca)

<sup>1</sup>Department of Electrical, Computer, and Biomedical Engineering, Ryerson University, Toronto, ON M5B 2K3, Canada.

<sup>2</sup>Department of Mechanical and Industrial Engineering, Ryerson University, Toronto, ON M5B 2K3, Canada.

This work was supported in part by the Natural Sciences and Engineering Research Council of Canada (NSERC) under Discovery Grants 2017-06930 and 2019-05562 and the Ryerson Faculty of Engineering and Architectural Science Dean’s Research Fund (FEAS DRF).

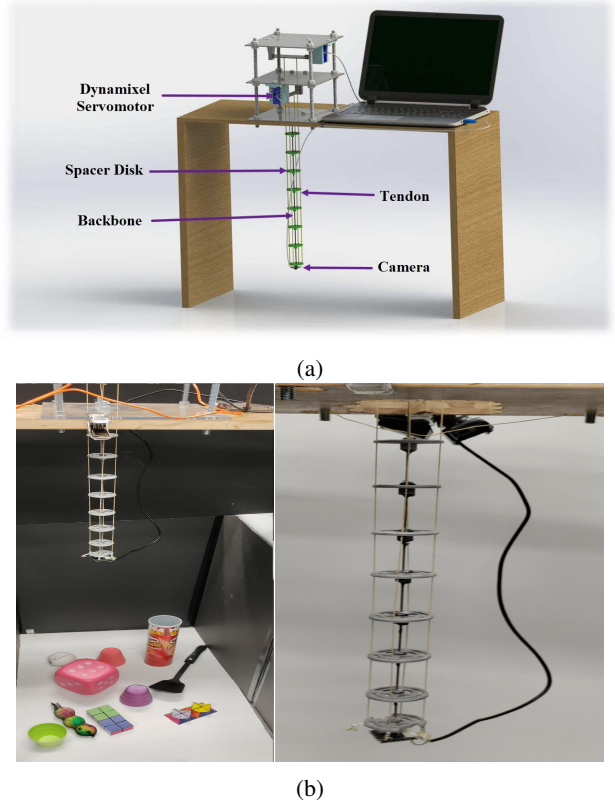


Fig. 1: (a) CAD model and (b) prototype of tendon-driven continuum robot. A sample of robot motion can be seen in the supplemented video.

[9] whereas another set focus on the model-free control approaches [10], [11]. The precise control of CRs always needs feedback on the state of the robot, including the position and velocity of the robot tip and also the shape of the robot. The feedback is often provided by physical sensors attached to the robot tip. This sensing method is the most common one in non-medical tasks, but medical scenarios limit them due to health-related issues, including biocompatibility and sterilizability of medical CRs, plus the essence of employing CRs that are water-resistant and insensitive to the temperature variance [12]. Therefore, non-contact sensing modalities such as vision-based methods find an important place in medical interventions. Further, vision-based methods can be easily implemented in medical applications where the imaging system is available in the field [13].

Vision-based control, also called visual servoing (VS), of CRs is a challenging problem among robotics researchers,

where the robot motion is controlled based on real-time visual feedback provided by one or more imaging devices. The error between the current visual information and the desired one, initially generated based on the desired scene, is calculated and fed to the controller to generate the control command for the robot's actuators. Depending on where the imaging device is positioned in the control loop to observe the scene of interest, VS has two paradigms called eye-in-hand (EIH) and eye-to-hand (ETH) [14]. In the former, the camera is mounted on the end-effector to observe the scene, whereas the latter requires the camera to be deployed in the environment on a fixed base to observe the scene of interest, including the robot.

Early methods of extracting visual information from the captured images were focused on geometric features such as points, lines, corners, edges, ridges, and blobs. Relying on these features, two basic approaches have been proposed and employed by the researchers, called image-based visual servoing (IBVS) and position-based visual servoing (PBVS) [14]. Wang *et al.* [15], [16] selected the IBVS-EIH approach for kinematic control of a cable-driven soft robot. They developed an adaptive PD tracking controller by knowing the intrinsic and extrinsic camera parameters, but they did not consider visual sensing accuracy in the modeling. Model-less optimal feedback control in the IBVS-ETH scheme was used by Yip *et al.* [17] to control a planar tendon-driven CR in the task space. They estimated the image Jacobian using backwards differencing. Zhang *et al.* [18] modeled the statics of a cable-driven parallel soft robot and implemented an open-loop/closed-loop switching controller in an IBVS-ETH scheme. The open-loop controller was developed based on finite element modeling in the simulation environment, which is computationally inefficient for real-time control.

Despite having several advantages, IBVS and PBVS have some disadvantages/limitations [14], [19]. The real-time pose estimation in PBVS schemes is always a challenge. The other significant challenge in the feature-based methods is that visual features should be extracted from a process that requires camera pose measurement, robust feature extraction, feature matching, and real-time tracking, all of which are complex and computationally heavy [20]. The success of the feature-based visual servoing, in fact, depends on the tracking success and performance, *i.e.*, the speed, accuracy, robustness, and redundancy of the visual features [21].

Using non-geometric VS, also called direct visual servoing (DVS), is an alternative to eliminate the feature tracking requirement. Photometric VS [22], as a DVS method, is a solution to the problem in a 2-dimensional (2D) scenario. It exploits the full image as a whole, uses the luminance of all pixels in the image, and avoids extracting geometric image features. Due to the redundancy of visual information in the control loop, DVS schemes are more accurate and robust than geometric feature-based VS methods [23]. Although these methods eliminate the feature extraction requirement, their convergence is inferior to that of the classical VS methods [24]. The reason is that there are nonlinear relations between the image information and the robot's 3-dimensional (3D)

motion.

One way of tackling this problem was proposed by Bateux *et al.* [24], [25], which is taking advantage of deep neural networks in image feature extraction and pose estimation. In this method, a convolutional neural network (CNN) was trained with the images captured from different scenes of an intended object and the corresponding pose of each image. The trained network was then employed to estimate the relative pose of the object seen by the camera. The target performed a highly precise, robust, and real-time 6-DOF PBVS of a rigid robotic manipulator. As an advantage, the proposed method does not necessarily need creating a new CNN because the user can re-purpose an existing pre-trained network tailored for a task close enough to the intended scenario. Also, the algorithm performed well on a scene that has never been seen at the training step [25]. This advantage enables the user to work on the generalization of the proposed CNN-based PBVS for a range of indoor and outdoor scenes that possess different illumination ranges. Felton *et al.* [26] proposed using a deep network for end-to-end DVS where the velocity of a camera mounted on a robot tip is predicted using a Siamese network. For training, they used a selected subset of the ImageNet dataset and evaluated the algorithm's performance on a 6-DOF rigid robot. Despite introducing several advantages, the approaches presented in [24]–[26] were not implemented on CRs, where tackling the control issue is a significant challenge. This research gap then motivated us to extend the benefits of their works, propose an end-to-end control approach, and evaluate the algorithm's performance and robustness experimentally.

The objective of this paper is developing the first deep learning-based kinematic control of continuum robots utilizing DVS methods and its implementation in joint space. The deep network is used to extract the current joint space variables of the CR corresponding to the captured images, and then controlling the robot by a proportional controller. The contributions of our work are:

- Developing a deep learning-based direct VS algorithm. The deep network is structured by repurposing a pre-trained VGG-16 network. The network is re-trained using a self-provided dataset (generated by Blender software), which includes variations of only one target image with normal conditions, illumination changes, and occlusions.
- Conducting extensive simulation studies in Blender in normal and perturbed conditions and then evaluating the controller's performance on a real robot. The algorithm is experimentally validated in a variety of scenarios including normal operation of the robot within the full range of its workspace. The robustness is also analyzed against variations of the lighting in the environment and partial occlusion.

The remainder of the paper is organized as follows. Section II presents the methodology of the research by stating the control law, describing the deep network architecture, and introducing the simulation environment and the train-

ing steps. The intended scenarios are first simulated and then experimentally validated in Section III. The results of the normal scenarios plus the robustness analyses are also presented in this section. Section IV, finally, concludes the article and briefly proposes future directions.

## II. METHODOLOGY

There exist many challenges in implementing VS on CRs. Unlike rigid robots with stable designs and well-defined kinematic models, the flexibility and soft nature of CRs make them susceptible to various modeling inaccuracies and extremely sensitive to noise and disturbance. Therefore, regressing the desired camera velocity is not sufficient for accurate control of CRs. Examples of uncertainties include extreme hysteresis, backlash, dead zone, and high sensitivity to disturbance. To combat these uncertainties, we propose a joint space VS scheme to localize the end-effector at a target image frame. This is achieved by implementing an end-to-end deep learning model that directly computes the desired tendon velocities from camera images. In order to robustly train the model, a simulation environment is created to generate a robust training dataset.

Our methodology is based on employing a deep learning network that has been already trained but repurposing it by changing the last layer and tailoring it for the desired task. Using the target image and the image frames captured in real time by a camera, the network produces the raw velocity commands that can direct the robot to the desired target after a subsequent scaling by a proportional controller. The intended network is trained using a user-generated dataset of RGB images produced utilizing Blender software. The performance of the proposed method is evaluated through extensive simulation and experimental studies in normal and changing conditions to prove that the algorithm is robust against lighting changes and partially occluded environments.

### A. Prototype Design and Development

As shown in Fig. 1a, the prototype CR has one section comprised of a flexible backbone made of spring steel, four braided Kevlar lines as tendons, and spacer disks to route the tendons. The tendons were placed around the backbone with an offset of  $1.8\text{ mm}$  and angular distance of  $90^\circ$  from each other. The tendons were routed toward the robot tip by eight equally distanced spacer disks, which were 3D printed using PLA filament. The disks were solidly attached to the backbone using steel-reinforced epoxy adhesive with a strength of  $3960\text{ psi}$ . A custom fixture was 3D printed to rigidly mount a USB camera on the robot tip in an EIH mode. The fixture was screwed on the last spacer disk such that it guarantees the minimum space between the camera and the robot tip while having no contact between the fixture and the camera’s electronic board. The tendons were actuated using Dynamixel AX-12A servomotors (Robotis, CA, USA). Table I shows the prototype specifications.

TABLE I: Prototype specifications.

Prototype’s Part	Specification	Value
Backbone	Density ( $\rho$ )	$7800\text{ Kg/m}^3$
	Young’s modulus ( $E$ )	$207\text{ GPa}$
	Length ( $L$ )	$0.4\text{ m}$
	Radius ( $r$ )	$0.9\text{ mm}$
Tendon	Breaking strength	$31.75\text{ Kg}$
USB camera	Frame rate	$30\text{ fps}$
	Resolution	$640 \times 480\text{ pixels}$
	Field of view (FOV)	$19^\circ$

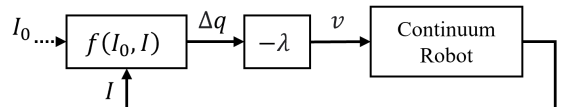


Fig. 2: Block diagram of the proposed visual servo controller comprised of a camera in an EIH mode, a tendon-driven CR, and a CNN model that takes the target image,  $I_0$ , and current image frame,  $I$ , and outputs desired tendon displacements,  $\Delta q$ , to be scaled by a control gain,  $-\lambda$ , and generate velocity command,  $V$ , for the robot drivers.

### B. Control Law

Classical VS approaches require complex Jacobian mapping, which is difficult to derive. Therefore, we aim to replace the entire mapping from image space to joint space with a learned model. Given an input image, the proposed model will output candidate velocities of each tendon such that the error between the current image frame,  $I$ , and the desired image frame,  $I_0$ , will be minimized to zero. As shown in Fig. 2, the output is multiplied by a gain,  $-\lambda$ , and fed into the CR. The gain adjusts the speed of the CR during experimentation. The larger the gain, the more aggressive the controller is in minimizing the error. The control law is then stated as

$$v = -\lambda f(I_0, I) \quad (1)$$

where  $v$  is the tendon velocity in  $\text{mm/s}$ ,  $\lambda$  is the control gain,  $I_0$  is the target image,  $I$  is the current image, and  $f()$  is a function of the target and current images implemented on a modified VGG-16 network to output  $\Delta q$ .

### C. Neural Network Design

In order to design an efficient neural network for our purpose, we utilized a VGG-16 backbone pre-trained on ImageNet to facilitate transfer learning [27]. Having been trained on natural images, only the lower layers of the network will need to be trained to regress desired tendon velocities. For our model, the first 10 layers were frozen to speed up the training as they already contain low-level features from natural images. We modified this network by dropping out the last dense layer and replacing it with a dense layer with two outputs corresponding to  $q_1$  and  $q_2$ . The activation function was set to linear (see Fig. 3). Various alternatives were considered to challenge this proposed model. Firstly, different backbones were considered, particularly ResNet50 and ResNet101. Secondly, we considered adding multiple

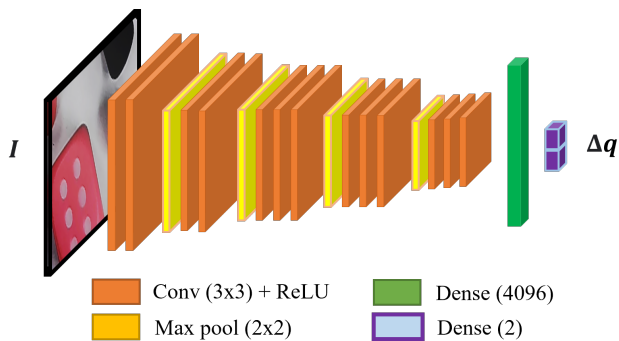


Fig. 3: Architecture of modified VGG-16 model.

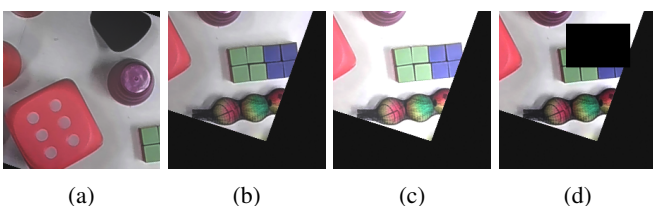


Fig. 4: Typical set of images used in simulation. (a) target image, (b) camera view at the tendon displacement of  $(q_1, q_2) = (4, -3) \text{ mm}$ , (c) camera view with random lighting, and (d) camera view with occlusion.

dense layers to improve the nonlinear fitting of the CR model. However, the added dense layers resulted in the loss of spatial awareness, which is key to our proposed model [28].

#### D. Simulation Environment

Training in the simulation provides various advantages over the real world. Not only are they much quicker in acquiring the data, but they also offer the opportunity to structure the environment to account for various noises and uncertainties, enabling the model to be more robust. On the contrary, attempting to learn the dynamics and uncertainties of the robot remains challenging in simulated environments. We resolved this problem by utilizing an open-source 3D computer graphics software called Blender and creating an environment that models the pose of the end-effector given a tendon displacement,  $q$ , value. This was achieved by using the forward kinematics of the robot to place and orient the virtual camera in the simulated environment. Being a single-section 2-DOF CR, we modeled the kinematics based on the constant curvature assumption, as presented by Rao *et al.* [29].

Whereas this approach ignores the dynamic effects of the CR, we propose that implementing robust vision control would allow the feedback loop to correct for most of the aforementioned challenges of the CR. Shadowing and occlusion were included to provide this robustness. Shadowing was achieved by adjusting the light source in the environment, whereas occlusion was achieved by placing black rectangles of random positions and dimensions within the image. Fig. 4 shows some samples from the simulation.

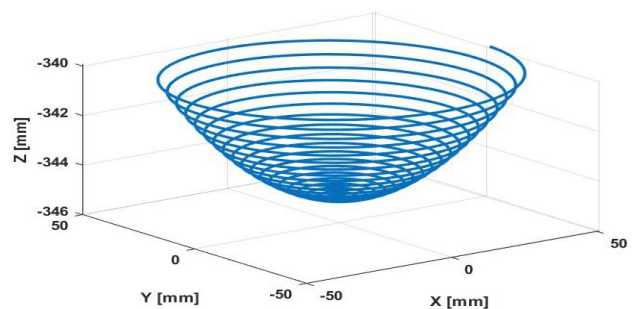


Fig. 5: Camera path used to generate the dataset. Assuming the camera is exactly mounted on the robot's tip,  $(x, y, z)$  are the coordinates of the camera's center point with respect to the robot's base.

For acquiring the dataset, previous approaches made use of two sets of images; one randomly placed within a distance from the origin for general convergence, and the other one very close to the origin for fine-tuning [25]. We thought this binary approach would produce noisier joint commands, and therefore we implemented a continuous method. The farther the CR is away from the origin, the sparser the dataset is. Similarly, to produce more deterministic results, a spiral path was used to traverse all reaching points in the 3D world within a certain threshold. The intended path can stimulate nonlinearities of the robot very well while covering all quadrants of the robot's workspace, which is of our interest in experiments. The spiral path was generated using

$$q_1 = \frac{A}{n} x \cos\left(\frac{P}{n} x * 2\pi\right) \quad (2)$$

$$q_2 = \frac{A}{n} x \sin\left(\frac{P}{n} x * 2\pi\right) \quad (3)$$

where  $A$  is the maximum displacement of the tendon,  $P$  is the total number of periods the CR makes,  $n$  is the number of sample points, and  $x$  is integers from 1 to  $n$ . Fig. 5 shows the generated spiral path. Using Blender, we created the environment and overlaid the desired scene. Employing a Python API, we moved the camera and light source around and captured images from the scene for training purposes.

#### E. Training and Validation

For training, we selected mean squared error (MSE) as the loss function because we designed our output activation function as linear. The ground truth of the dataset was generated based on equation (4), which keeps the ground truth between  $-1$  and  $1$ , allowing for better training.

$$q_{new} = \tanh(10q) \quad (4)$$

In comparison, we linearly mapped  $-5 \text{ mm}$  and  $5 \text{ mm}$  to  $-1$  and  $1$ , respectively, clipping any values beyond. However, such an approach would not penalize the optimizer as much near the origin. Since we aim to propose sub-millimeter accuracy, utilizing equation (4) would force convergence while producing a much smoother velocity profile.

The simulation environment was used to generate the dataset. To this end, 5000 images were acquired with a maximum amplitude of  $7\text{ mm}$  and a period of 20. Random lighting effect and random occlusion were included. These occlusions were represented as black rectangles overlaid at random positions to force the model to learn the full spatial features and make it more robust. As we used the classical VGG-16, the input image was RGB of size  $224 \times 224$ . The model was trained for 50 epochs with a batch size of 32 and a learning rate of  $1e-5$  using Adam optimizer. The final MSE was determined to be  $3e-5$ . To validate our hypothesis, VGG-16 was swapped with ResNet51 and ResNet101. As expected, the training took substantially longer, and the MSE was inferior to that of the VGG. Similarly, two dense layers (1024 and 512, respectively) were added between the VGG and the final  $q$  output to test our hypothesis. Nonetheless, the training took longer without any significant improvement to the MSE. Training on an Nvidia Titan Xp GPU was reasonably fast, taking less than 20 minutes on 50 epochs to train. The model inference was also extremely fast, taking about  $15\text{ ms}$  per frame<sup>1</sup>.

### III. EXPERIMENTAL RESULTS

#### A. Simulation

Before conducting experiments in real-world scenarios, we performed some tests to validate the robustness and accuracy in simulation. Since the kinematics did not incorporate nonlinear effects when generating the dataset, we needed to include various uncertainties to prove the model's robustness within the simulation.

1) *Modeling Uncertainties*: Since the constant curvature assumption does not hold true in all situations, other uncertainties and disturbances were added to the simulation. Regarding geometric uncertainties, deriving from parameters of the robot including length, disks space, etc., Gaussian noise with a mean of 0 and standard deviation of  $0.01\text{ mm}$  was added to the output  $q$  values. Also, the outputs of the trained model were scaled to uniformly distributed random numbers in the range of 0.25 to 4. Random lighting was introduced to account for the vision uncertainties, and a region within the image was occluded with black rectangles. Instead of generating these random scene environments every iteration, we chose to regenerate these random uncertainties every 20 iterations to better model the changing conditions of the real-world environment.

2) *Simulation Results*: Simulating with the initial tendon displacements of  $(q_1, q_2) = (6, -4)\text{ mm}$  we noticed the CR is able to converge smoothly although less than 25% of the target image was visible at the starting position. Moreover, the change in lighting, as shown in Fig. 6, did not impact the convergence of the CR. More interestingly, adding occlusion (at times greater than 80%) did not destabilize the CR and, as noted with the raw network output in Fig. 7, was still able to counteract the Gaussian noise added to the actuation

<sup>1</sup>The code and dataset will be made available publicly once the paper is accepted.

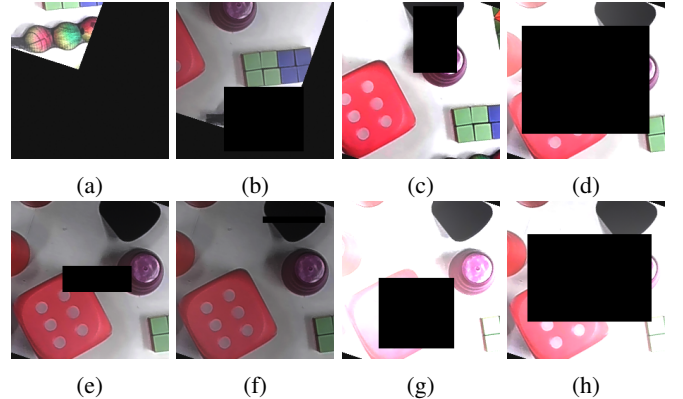


Fig. 6: Sequence of camera views in a typical simulation started at the tendon displacement of  $(q_1, q_2) = (6, -4)\text{ mm}$  at iteration numbers of (a) 1, (b) 25, (c) 50, (d) 75, (e) 100, (f) 225, (g) 250, and (h) 299.

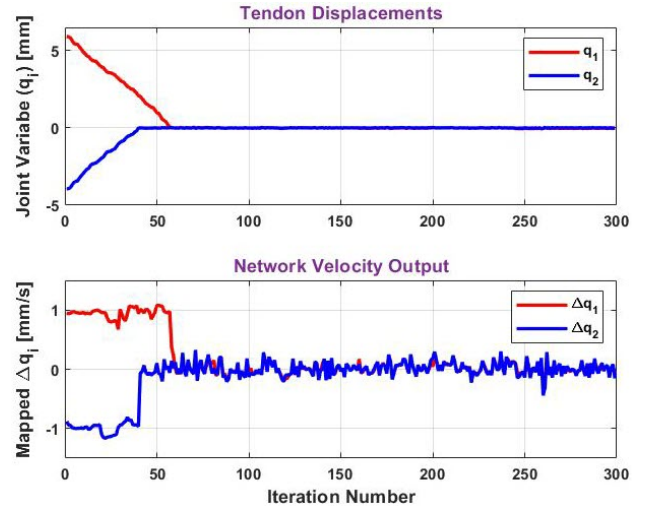


Fig. 7: Tendon displacement (top) and raw velocity commands from the network, before being multiplied by  $-\lambda$ , to stabilize the robot (bottom).

commands of the CR. A sample of simulation studies can be seen in the supplemented video. Having successfully validated in simulation, the next section will extend it to the real-world environment.

#### B. Experimental Validation

In order to test the practicality of the proposed end-to-end model, we applied it to the experimental setup developed for the purpose to showcase its robustness to various noises and uncertainties. Fig. 1b shows the prototyped robot for the experiment.

1) *Experiment Design*: The physical environment was structured similar to the simulation environment, as shown in Fig. 1b. To test the model's accuracy in converging the CR, the end-effector was moved to random positions, and the trained model attempted to minimize the difference between the current image frame  $I$  to the target image  $I_0$  on which the model has been trained. The range of motion was limited

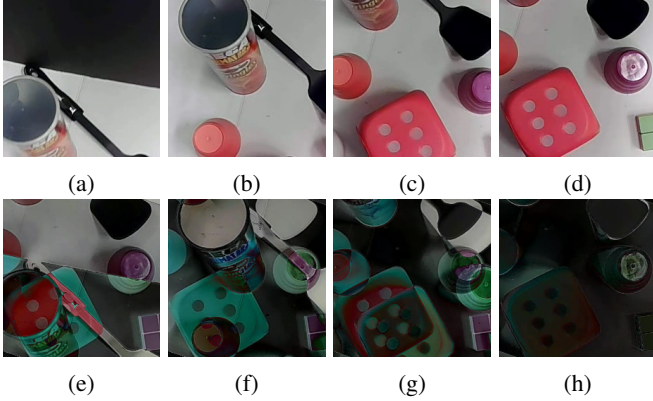


Fig. 8: (a-d) Sequence of camera views in a typical experiment started at the tendon displacement of  $(q_1, q_2) = (5, -7) mm$ , (e-h) Corresponding difference between the normalized target and intended images.

to  $\pm 10 mm$  for each tendon to keep the scene within the camera's field of view (FOV). Note that the scene with which the model was trained on was larger than the camera's FOV, which enabled our model to operate despite there being no overlap with the target image. In addition, to show the robustness of the controller, the robot was operated in dynamic lighting conditions, dynamic occlusion and finally partial static occlusions.

2) *Results and Discussion*: Experimenting from the initial tendon displacements of  $(q_1, q_2) = (5, -7) mm$ , the first row in Fig. 8 shows that the CR converges to match the camera image to the target image. Normalizing and then subtracting the current and target images gives the images on the second row. Upon convergence, the overlap between the two images becomes highly precise. To evaluate the convergence quantitatively, the sum of absolute distance (SAD) between the normalized target and current image was calculated using

$$SAD = \sum |I^* - I_0^*| \quad (5)$$

where  $I^*$  is the normalized current image and  $I_0^*$  is the normalized target image. As shown in Fig. 9, the SAD value fails to approach zero, stating that the lighting environment and image exposure were slightly different.

Note that  $q_1$  and  $q_2$  values do not approach 0 in Fig. 9 despite that being the origin with which the target image was taken. This can be assigned to the dynamic effects of the CR and, more specifically, its hysteresis, which will be addressed in our future research. Without the need for a computationally complex controller, our model can converge the camera frame to the target image by automatically compensating for the nonlinear effects. The raw velocity commands show that the model smoothly converges to the origin and stabilizes once it approaches.

In order to test the robustness, different lighting conditions and occlusions were considered. As seen in Fig. 10, the top row images show the CR at the starting position,  $(q_1, q_2) = (-2, 2) mm$ . The left columns show the dynamic lighting scenario, the center column shows the dynamic occlusion

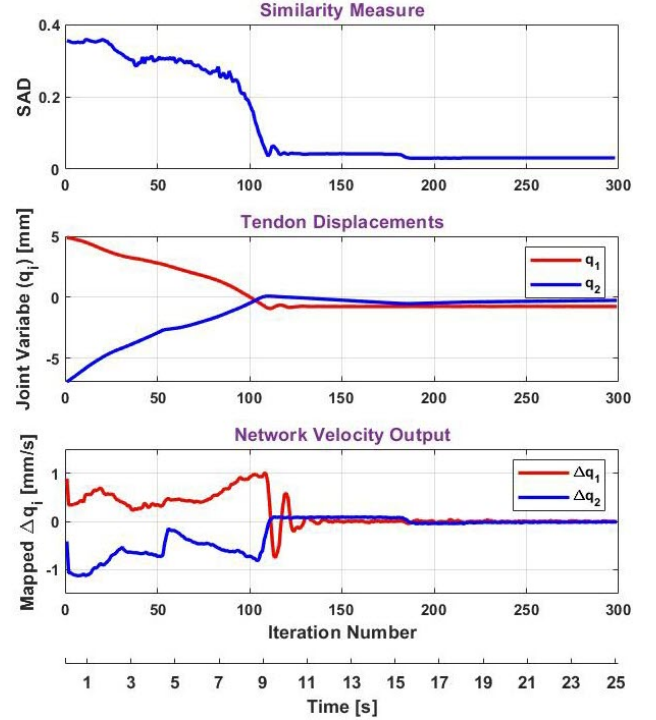


Fig. 9: SAD between  $I^*$  and  $I_0^*$  (top), tendon displacement at each iteration (middle), and the raw velocity commands, before being multiplied by  $-\lambda$ , from the network to stabilize the robot (bottom).

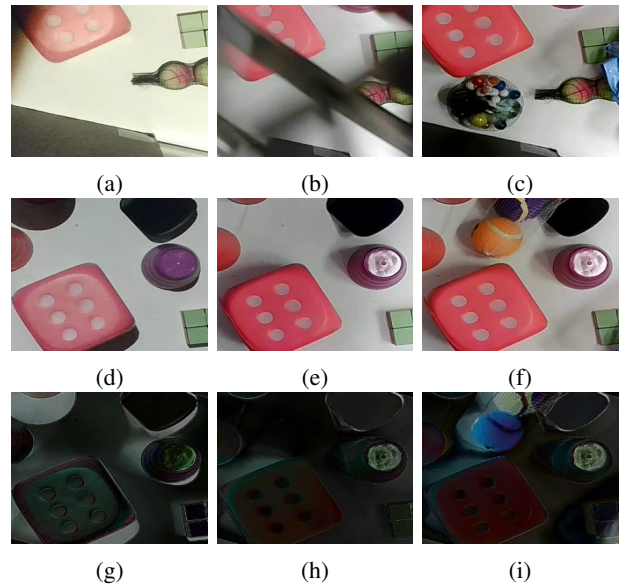


Fig. 10: (a-c) Initial views of the camera in the robustness analyses using dynamic lighting, dynamic occlusion, and partial static occlusion, respectively. (d-f) Corresponding converged views. (g-i) Corresponding difference between the target image and converged views.

scenario, and the right column shows static partial occlusion scenario. The bottom row shows the corresponding normalized differences with the target image at the final iteration for each scenario. Despite the uncertainties, the precise overlap confirms that the model has learned sufficiently through simulation alone and that it can robustly control the CR in an end-to-end fashion. Note that even though the simulation only used one 2D image of the target scene, which results in projection artifacts when simulating in 3D, the model successfully operated in the real 3D environment. Four samples of experimental validation and robustness analysis can be seen in the supplemented video.

#### IV. CONCLUSION AND FUTURE WORK

In this paper, a deep direct visual servoing algorithm was proposed to control a single-section tendon-driven continuum robot in an eye-in-hand mode. The algorithm takes one image from the target and trains a modified VGG-16 network by generating a dataset using Blender software. The dataset includes different views of the scene plus illumination change and occlusion for robustness analysis. The algorithm was tested on a real robot developed by the team and showed good efficiency by fast and accurate convergence in normal scenes. Also, the algorithm's robustness was pursued in scenarios incorporating dynamic illumination changes as well as dynamic and static occlusions. In all robustness analysis tests, the algorithm managed to control the robot effectively and efficiently.

Despite the good convergence rates we obtained, the research will be extended in our future work. The robot will be extended to multi sections, and the dynamic effects of the robot motion such as hysteresis, tendon slack, backlash, dead zone, and external disturbances will be investigated. We expect to include a nonlinear controller for future steps as dynamic uncertainties require us to consider different phenomena affecting the robot movements.

#### REFERENCES

- [1] I. D. Walker, "Continuous backbone "continuum" robot manipulators," *International Scholarly Research Notices*, vol. 2013, pp. 1–19, 2013.
- [2] A. A. Nazari, D. Castro, and I. S. Godage, "Forward and inverse kinematics of a single section inextensible continuum arm," *arXiv preprint arXiv:1907.06518*, 2019.
- [3] D. B. Camarillo, C. F. Milne, C. R. Carlson, M. R. Zinn, and J. K. Salisbury, "Mechanics modeling of tendon-driven continuum manipulators," *IEEE Transactions on Robotics*, vol. 24, no. 6, pp. 1262–1273, 2008.
- [4] R. Qi, A. Khajepour, W. W. Melek, T. L. Lam, and Y. Xu, "Design, kinematics, and control of a multijoint soft inflatable arm for human-safe interaction," *IEEE Transactions on Robotics*, vol. 33, no. 3, pp. 594–609, 2017.
- [5] E. Amanov, T.-D. Nguyen, and J. Burgner-Kahrs, "Tendon-driven continuum robots with extensible sections—a model-based evaluation of path-following motions," *The International Journal of Robotics Research*, vol. 40, no. 1, pp. 7–23, 2021.
- [6] R. J. Webster, A. M. Okamura, and N. J. Cowan, "Toward active cannulas: Miniature snake-like surgical robots," in *2006 IEEE/RSJ International Conference on Intelligent Robots and Systems (IROS)*. IEEE, 2006, pp. 2857–2863.
- [7] H. B. Gilbert, D. C. Rucker, and R. J. Webster III, "Concentric tube robots: The state of the art and future directions," in *Robotics Research: The 16th International Symposium ISRR*. Springer International Publishing, 2016, pp. 253–269.
- [8] J. Burgner-Kahrs, D. C. Rucker, and H. Choset, "Continuum robots for medical applications: A survey," *IEEE Transactions on Robotics*, vol. 31, no. 6, pp. 1261–1280, 2015.
- [9] M. Chikhaoui and J. Burgner-Kahrs, "Control of continuum robots for medical applications: State of the art," in *ACTUATOR 2018; 16th International Conference on New Actuators*. VDE, 2018, pp. 1–11.
- [10] T. George Thuruthel, Y. Ansari, E. Falotico, and C. Laschi, "Control strategies for soft robotic manipulators: A survey," *Soft Robotics*, vol. 5, no. 2, pp. 149–163, 2018.
- [11] T. da Veiga, J. H. Chandler, P. Lloyd, G. Pittiglio, N. J. Wilkinson, A. K. Hoshiar, R. A. Harris, and P. Valdastrì, "Challenges of continuum robots in clinical context: a review," *Progress in Biomedical Engineering*, vol. 2, no. 3, p. 032003, 2020.
- [12] A. A. Nazari, F. Janabi-Sharifi, and K. Zareinia, "Image-based force estimation in medical applications: A review," *IEEE Sensors Journal*, vol. 21, no. 7, pp. 8805–8830, 2021.
- [13] M. M. Fallah, S. Norouzi-Ghazbi, A. Mehrkish, and F. Janabi-Sharifi, "Depth-based visual predictive control of tendon-driven continuum robots," in *2020 IEEE/ASME International Conference on Advanced Intelligent Mechatronics (AIM)*. IEEE, 2020, pp. 488–494.
- [14] S. Hutchinson, G. D. Hager, and P. I. Corke, "A tutorial on visual servo control," *IEEE Transactions on Robotics and Automation*, vol. 12, no. 5, pp. 651–670, 1996.
- [15] H. Wang, W. Chen, X. Yu, T. Deng, X. Wang, and R. Pfeifer, "Visual servo control of cable-driven soft robotic manipulator," in *2013 IEEE/RSJ International Conference on Intelligent Robots and Systems (IROS)*. IEEE, 2013, pp. 57–62.
- [16] H. Wang, B. Yang, Y. Liu, W. Chen, X. Liang, and R. Pfeifer, "Visual servoing of soft robot manipulator in constrained environments with an adaptive controller," *IEEE/ASME Transactions on Mechatronics*, vol. 22, no. 1, pp. 41–50, 2016.
- [17] M. C. Yip and D. B. Camarillo, "Model-less feedback control of continuum manipulators in constrained environments," *IEEE Transactions on Robotics*, vol. 30, no. 4, pp. 880–889, 2014.
- [18] Z. Zhang, T. M. Bieze, J. Dequidt, A. Kruszewski, and C. Duriez, "Visual servoing control of soft robots based on finite element model," in *2017 IEEE/RSJ International Conference on Intelligent Robots and Systems (IROS)*. IEEE, 2017, pp. 2895–2901.
- [19] F. Janabi-Sharifi, L. Deng, and W. J. Wilson, "Comparison of basic visual servoing methods," *IEEE/ASME Transactions on Mechatronics*, vol. 16, no. 5, pp. 967–983, 2010.
- [20] É. Marchand and F. Chaumette, "Feature tracking for visual servoing purposes," *Robotics and Autonomous Systems*, vol. 52, no. 1, pp. 53–70, 2005.
- [21] M. Ourak, B. Tamadazte, O. Lehmann, and N. Andreff, "Direct visual servoing using wavelet coefficients," *IEEE/ASME Transactions on Mechatronics*, vol. 24, no. 3, pp. 1129–1140, 2019.
- [22] C. Collewet and E. Marchand, "Photometric visual servoing," *IEEE Transactions on Robotics*, vol. 27, no. 4, pp. 828–834, 2011.
- [23] L.-A. Duffot, R. Reichenhofer, B. Tamadazte, N. Andreff, and A. Krupa, "Wavelet and shearlet-based image representations for visual servoing," *The International Journal of Robotics Research*, vol. 38, no. 4, pp. 422–450, 2019.
- [24] Q. Bateux, E. Marchand, J. Leitner, F. Chaumette, and P. Corke, "Visual servoing from deep neural networks," *arXiv preprint arXiv:1705.08940*, 2017.
- [25] —, "Training deep neural networks for visual servoing," in *2018 IEEE International Conference on Robotics and Automation (ICRA)*. IEEE, 2018, pp. 3307–3314.
- [26] S. Felton, E. Fromont, and E. Marchand, "Siame-se(3): regression in se(3) for end-to-end visual servoing," in *2021 IEEE International Conference on Robotics and Automation (ICRA)*. IEEE, 2021, pp. 14454–14460.
- [27] K. Simonyan and A. Zisserman, "Very deep convolutional networks for large-scale image recognition," *arXiv preprint arXiv:1409.1556*, 2015.
- [28] A. Kendall, M. Grimes, and R. Cipolla, "Posenet: A convolutional network for real-time 6-dof camera relocalization," in *2015 IEEE International Conference on Computer Vision (ICCV)*. IEEE, 2015, pp. 2938–2946.
- [29] P. Rao, Q. Peyron, S. Lilge, and J. Burgner-Kahrs, "How to model tendon-driven continuum robots and benchmark modelling performance," *Frontiers in Robotics and AI*, vol. 7, pp. 1–20, 2021.